The role of the internal capacitance in organic memristive device for neuromorphic and sensing applications.

*Silvia Battistoni, Matteo Cocuzza, Simone Luigi Marasso, Alessio Verna, Victor Erokhin**

Dr. Silvia Battistoni, Prof. Matteo Cocuzza, Dr. Simone Luigi Marasso, Dr. Victor Erokhin Consiglio Nazionale delle Ricerche, Institute of Materials for Electronics and Magnetism (CNR-IMEM), Parma, Italy
Email Address: victor.erokhin@imem.cnr.it
Prof. Matteo Cocuzza, Dr. Simone Luigi Marasso, Dr. Alessio Verna
Chilab—Materials and Microsystems Laboratory, DISAT, Politecnico di Torino, Chivasso (Turin), Italy

Keywords: *Organic memristive devices, Biosignals, Neuromorphic Devices*

Organic electronics has recently emerged as promising candidate for the emulation of brain-like functionalities, especially at the device level. Among the proposed technologies, memristive devices have gained an increasing attention due to their non-volatile behaviour, which makes them suitable for the implementation of artificial neuronal networks. However, most of them have an energy costly switching mechanism, which limits the approaching of brain like energy efficiency. Differently from them, organic memristive devices (OMDs) have a narrow switching window and implement neuromorphic characteristics at voltages ≤ 1V. Despite OMDs potentialities in bioinspired electronics, guidelines for the design of devices and materials are still missing. Here we show that the device capacitance represents a significant degree of freedom for targeting devices applications. We also show that a single OMD emulates activity dependent synaptic functions and neuronal temporal and spatial summation, taking advantage of its three-terminal configuration. Interestingly, despite the neuromorphic applications, OMDs can also sense and amplify incoming signals based on their capacitive and/or resistive values. This spectrum of applications, ranging from volatile to non-volatile characteristics and from neuromorphic computing to bio signals sensing, sets the stage for the realization of integrated circuits for adaptive sensing.

1 Introduction

Neuromorphic systems are widely considered as powerful alternatives for information storage and handling with respect to traditional computing systems which at the moment are unable to equal the brain capabilities in real world information processing [1].
The possibility of building integrated and complex neuromorphic systems has to deal with the integration between different brain functions. In brain, neurons are responsible for the temporal and spatial integration of incoming signals and for the signal propagation, while synapses are tasked with the variation of the input signal transmission according to learning paradigms such as the activity dependent plasticity (Long Term and Short Term Plasticity) or the Spike-Timing Dependent Plasticity (STDP) algorithm [2]. This structural and functional organization enables the energy efficient and the massively parallel information processing that characterize neuronal networks.
Artificial analogs of neurons and synapses can be implemented using traditional electronic elements fabricated with well-established CMOS technology [3, 4]. However, these implementations require the use of a rather large number of elements [5], limiting the effective realization of brain-like systems, especially considering the 3D organization and the possibility of rather long-distance connections. This is the reason why main efforts in the field of artificial neuron networks (one class of neuromorphic systems) were carried out mainly at the software level, limiting the mimicking of several features of brain, for instance parallel information processing.
Recently, a renovated interest in the hardware realization of neuromorphic systems and, in particular, artificial neuron networks [6, 7] is due to the progress achieved in the implementation of resistance switching elements [8, 9, 10], the so called memristive devices [11], mimicking synapse properties at the level of single elements and allowing the realization of neuron analogs. Different groups reported synaptic like devices using nanoscale magnetic materials developing spintronic devices [12, 13], metal oxides [14, 15, 16] or organic materials based on redox reactions [17, 18, 19] and ion permeation [20, 21, 22]. The increasing interest in organic materials demonstrating basic forms of neuroplasticity has recently driven the development of different approaches for reducing the operation voltage ranges [23, 24] and for increasing the networks density [25]. Short term memory and adaptation functions have been reported in different organic devices [26, 27, 28, 29], demonstrating the capability of performing paired pulse facilitation or depression (PPF or PPD, respectively), while spatio-temporal neuronal integration has been demonstrated in devices with a multi-gate configuration [27] or in NbO_x volatile memristors [30].
It has been recently proposed that a neuromorphic system integrated with a sensing part will be able to locally process data and to activate subsequent events [1]. In this interesting scenario, the lack of a technology able to integrate devices with different specific functions (sensing and neuromorphic computing) seems the major bottleneck.

The implementation of organic based synaptic elements based on polyaniline (PANI) is supported by its theoretical fast resistive switching [31], the marked difference between high and low resistance of partially oxidized and reduced states [32], the light weight and its electrochromic behavior. Indeed, PANI based organic memristive devices (OMDs) have demonstrated several advantages, including the flexibility, a high and finely controllable ON/OFF ratio and the possibility of monitoring the internal conductivity taking advantage of its electrochromism, instead of external electrical set up. Historically designed as synapse-mimicking electronic element, OMDs have been largely used in circuits and systems and recently it has been shown that the overlay of noise to the input signal can improve the devices characteristics, similarly to what occurs in nervous system [33]. Despite these advantages and interesting features, the realization of micro-OMDs (in which the channel dimensions are at the microscale) is relatively recent [34, 17]. Moreover, the impact of the device geometry on the fundamental mechanism behind their operation remains practically unexplored. Here we show that OMDs performances may be understood using as a key parameter the thin film capacitance that shows a linear dependency on volume and resistance of the PANI channel. This result provides guidelines for the design of devices. We also demonstrate that micro-OMDs owned a wide range of neuromorphic functions that embrace the emulation of synaptic long-term and short-term plasticity and the mimicking of neurons-like spatio-temporal integration activity. Furthermore, OMDs share their geometry with poly(3,4-ethylenedioxythiophene) doped with polystyrene sulfonate (PEDOT:PSS) based transistors (Organic ElectroChemical Transistors, OECTs) which find large use in bioelectronics as amplifying transducers. We show that, despite the native neuromorphic applications, OMDs may be employed as amplifying transducers for the recognizing of bio-signals. This possible field of application, mediated by the already mentioned capacitive thin film contribution, could possibly pave the way for the realization of sensing systems integrated with neuromorphic networks in which the same PANI based device is declined in different functions.

2 Results and Discussion

In OMDs, the PANI active layer is deposited in contact with two gold electrodes (Drain (D) and Source (S)) from which the channel current is monitored during the application of an external bias (V_{SD}). For the correct functioning of this type of memristive devices it is necessary to ensure the direct contact between the polymeric thin layer and the liquid electrolyte, in which a silver wire works as gate electrode (Figure 1a).The thickness of the PANI layer is controllable up to the nm scale, thanks to the selected deposition technique (the Langmuir Schaefer method), which allows the conformal deposition of single monolayer of polymers and small molecules (Figure 1b) on selected substrates. The channel current is a superimposition of the electronic current flowing in the PANI channel (I_{SD}), which depends on the internal conductivity of the polymer, and the ionic current (I_{GS}) flowing at the interface between PANI and the electrolyte, which depends on the external bias applied to OMD. This latter is to be considered as the expression of the redox activity of the conductive polymer on which the switching mechanism for this type of memristive devices is based on. In other words, the external bias voltage, applied to OMDs (V_{SD}), triggers the redox activity of the PANI channel which affects the instantaneous conductivity variation of the entire device (σ). The resulting current follows Equation 1:

$$I_{SD}(t, V_{SD}) = V_{SD}(t) * \sigma(t, V_{SD}) dW/L \quad (1)$$

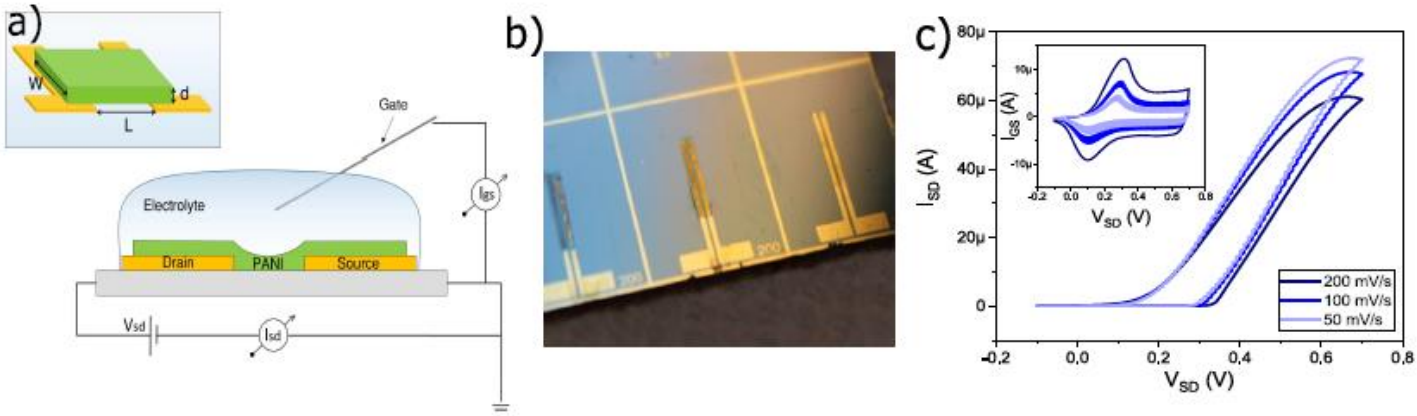

Figure 1 : Panel a) OMDs scheme and electrical configuration: gold Source and Drain electrodes are in contact with a polymeric thin film of polyaniline (PANI). This latter is in direct contact with an electrolytic solution in which a silver wire is inserted as gate electrode. Source and Drain electrodes are biased with V_{SD} voltage value, which induces resistivity variations in I_{SD} and I_{GS} currents. In the inset, geometrical details of length (L), thickness (d) and width (W); Panel b) image of the PANI active layer; Panel c) I_{SD} response to V_{SD} variations as a function of the scan speed. In the inset relative I_{GS} responses.

where d, W and L are the thickness, the width and the length of the PANI layer (inset of Figure 1a). Despite the electrical dependence on the PANI conductivity which can vary of 5 orders of magnitude [31], this equation implies a reliance of the output current on the geometry of the device. To deepen this aspect, we realized and measured electrical responses of OMDs with PANI channels of different volumes varying the length between 10 and 200 *µm*, the width from 250 to 6000 *µm* and the nominal thickness from 10 to 60 monolayers (which correspond to a thickness range between 25 and 150 nm [35, 36]). OMDs typical cyclic voltage-current characteristic (Figure 1c) presents a marked hysteresis in the positive range of the voltage and a rectifying behaviour in the negative one, that is a reflection of the electrochemical reactions occurring in the PANI channel [17].The shape of the hysteresis depends on the scan speeds, pH condition [37] and on the channel geometry which affects the maximal accessible conductivity of the entire device. Varying the scan speed, the kinetics of PANI electrochemical reactions could be promoted or suppressed [38, 39] (inset of Figure 1c), resulting in a larger or smaller hysteresis loop in electrical characteristics (Figure 1c).

2.1 Time and capacitive response

Beside from electrochemical considerations, I_{GS} vs V_{SD} curves can be used for the estimation of the polymeric thin film capacitance [39, 38] (section 4.2.2). Obtained results are in a good agreement with already reported estimation of PANI OMD capacitive values [35] for pH 1. Reporting calculated results vs the PANI channel volume (Figure 2a), a well defined linear trend defines a capacitance per volumetric unit of $C=5.3 \pm 0.4 * 10^{-10}$ F/μm^3 = 528 ± 43 *F/cm*^{3}.
This volumetric capacitance is in agreement with the already reported PANI volumetric capacitance [35, 40, 41], but in any case is an order of magnitude higher with respect to the value obtained for another type of organic electrochemical devices (i.e. OECTs) [42] widely used in bio electronics for sensing applications. It has to be noted that despite the linearity with channel volume, PANI OMD capacitance shows a linear trend with the minimum resistance of the channel (Figure 2c). On the contrary, the switching times (τ in Figure 2b), measured following the procedure reported in the section 4.2.2, seems to have not a clear dependence on the volume or the capacitance of organic memristive devices and to be distributed around ≈ 0.2 *s* with an obtained minimum value of 65 ms (Figure 2b). These values, well below the already reported τ for analogous solid macrodevices [43] and solid microdevices [34] are in contrast with the predicted linearity between the switching time and the area of the OMD active channel reported in 2011 [35] and the theoretical switching time of PANI which is expected to be in the range of hundreds of *µs* [31]. It has to be noted that the linear trend proposed by Pincella et al.

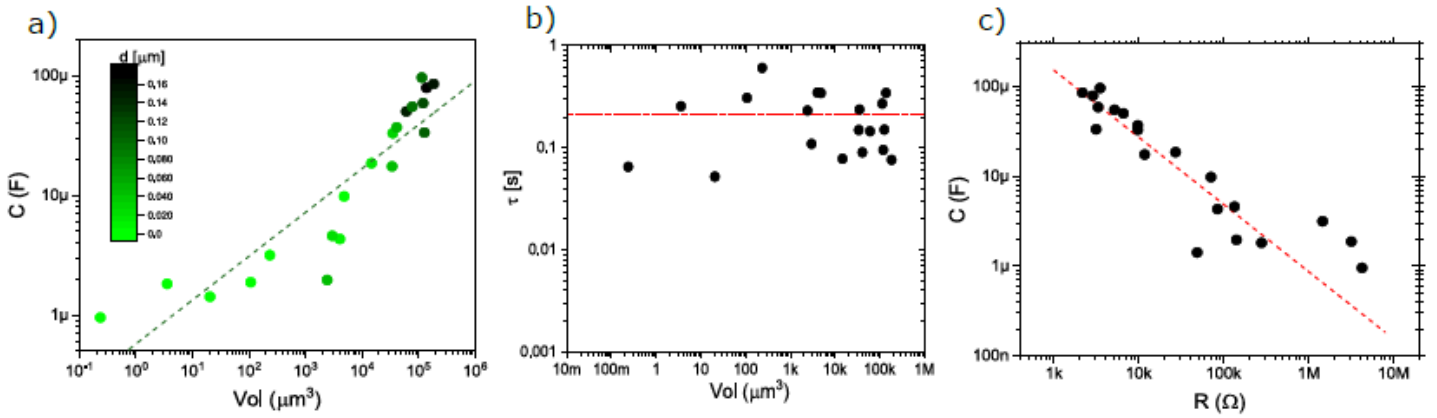

Figure 2: Panel a) Volumetric dependence of the device capacitance; panel b) Volumetric dependence of the OMDs switching time. Red dotted line is the mean value obtained from the normal distribution of switching times; panel c) Capacitance dependence on the PANI channel resistance.

was obtained employing macrodevices with switching times of the order of seconds, well above the here reported results. Moreover, in Lacroix et al. [31] this reduced switching time was obtained using another experimental configuration, in which the switching event occurred along the PANI thickness plane. In our case instead, it has been reported that PANI resistance switching is a dynamic process involving the entire volume of the polymeric channel which is exposed to a voltage distribution rather than a constant equipotential bias. To this geometrical consideration, we can compound the reported non-homogeneity of the film thicknesses for less than 10-15 transferred layers [36]. Therefore, we can infer that the combination of these effects deviates the obtained OMD switching time from the predicted PANI value.

2.2 Endurance and Number of Resistive States

To evaluate the stability of OMDs and the stability of their switching processes, we have carried out endurance tests on devices to determine the minimum number of cycles that memristive devices can endure (Figure 3a).

OMDs with different volumes (and thus with different calculated capacitance values) show different $(R_{OFF}-R_{ON})/R_{ON}$ as expected (Figure 3b): devices with higher C values have a larger relative variation between low and high resistance which progressively decreases with the reducing of the C values. In any case, this kind of organic memristive devices with liquid electrolyte have a stability of more than 10^3cycles with standard deviations within 6% (Figure 3a). This result is in line with already reported endurance tests performed on OMDs based on solid electrolytes[34], in which the device presented a rather stable switching between high and low conductivity level up to the 1000^{th} cycle and then started to present larger oscillations.

However, for the integration of OMDs with electronic bio-circuits, where their memorization capabilities must be effectively employed, it is necessary to assess the number of resistance states of organic memristive devices. In OMDs this can be accomplished by applying voltage pulses of fixed dwell time (Δt) and increasing amplitude (V_p) (Figure 3c) or by applying voltage pulses with a fixed amplitude and varying the dwell time (Figure 3d). Both these stimulation schemes efficiently increase the OMD internal conductivity (as indicated in relative figures with red stars), inducing current variations proportional to the voltage amplitude in the first case and to the dwell time in the second.

To estimate the number of resistive states, we decided to follow the procedure with increasing amplitude voltage pulses and we applied to OMD a train of stimuli with 0.3 $V < V_p < 0.89$ V with steps of 10 mV. As shown in Figure 3e, OMDs discriminate pulses of voltage separated by 10 mV and they can access to 52 different internal resistance states (calculated as $\Delta I_{SD} = I^f_{SD} - I^0_{SD}$ where I^f_{SD} and I^0_{SD} are the final and the initial current levels after and before the V_p application- Figure 3f), which correspond to a memory with more than 5.5 bits. It is worth noticing that all the tested samples show a minimum of 39 states (5 bits) and this result is of particular relevance if considering the actual record of 6.5 obtained

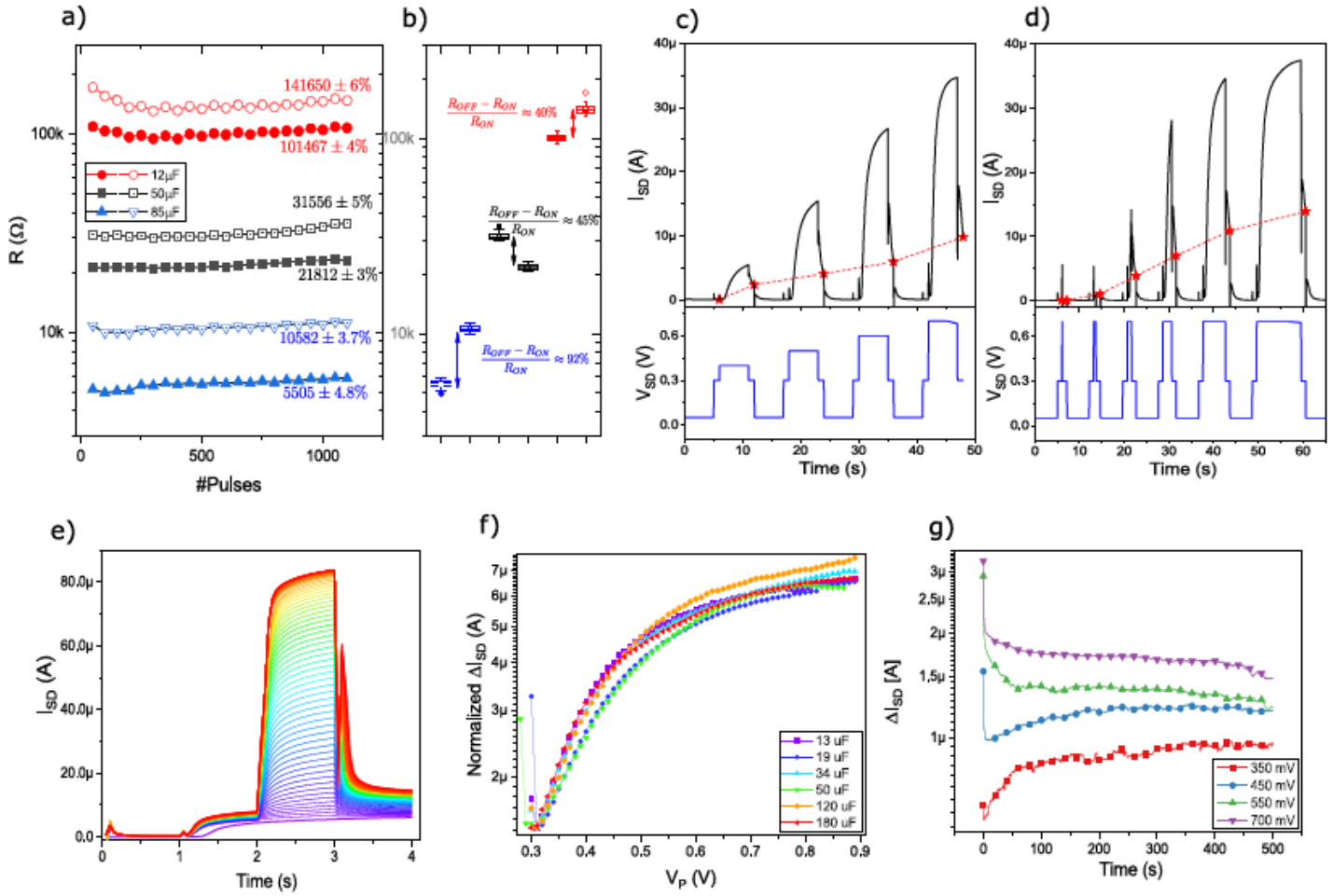

Figure 3: Panel a) Endurance test: evolution of the high and low resistance as a function of the number of switch cycles for devices with different capacitive values; panel b) Means and standard deviations of panel a); Panels c and d) Increment of the conductivity as a function of the voltage pulses amplitude (panel c) or of the pulse dwell time (panel d); panel e) Number of resistance states: typical I_{SD} vs time for voltage pulses with amplitude 0.3 V ≤ Vp ≤ 0.89 V with steps of 10 mV; panel f) evolution of the resistance states vs Vp for different devices' capacitances; panel g) temporal evolution of selected resistance states.

by Stathopoulos et al. with metal-oxide memristive devices[44]. This behaviour is independent from device's capacitive values (Figure 3f) and shows an initial linear evolution of the internal states with respect to V_p followed by a saturation regime. We further assessed the stability of these resistivity states by monitoring their temporal evolution up to $5x10^2$s (Figure 3g).

2.3 Neuromorphic properties

OMDs are well known neuromorphic devices thanks to their ability of adjusting the internal resistivity with the amount of charge that passed through them. More in detail, macrodevices have demonstrated to be able to implement activity dependent functions [45] while solid microdevices successfully demonstrated the implementation of STDP[46]. Liquid microdevices with the already mentioned faster switching kinetics are predicted to exhibit the same neuromorphic functions of previously reported devices, closing the gap

between devices and synapses temporal scales. To evaluate OMDs neuromorphic capabilities, we tested them following already adopted protocols[45] for the synaptic activity dependent functions (i.e. Long Term and Short Term Potentiation and Depression- LTP, LTD and STD and STP respectively) and we explored new neuronal functions of spatial and temporal integration. In line with the results reported on macrodevices, a train of voltage pulses (V_p=700 mV,Δt=100 ms) delivered to OMDs following the scheme reported in the inset of Figure 4d,

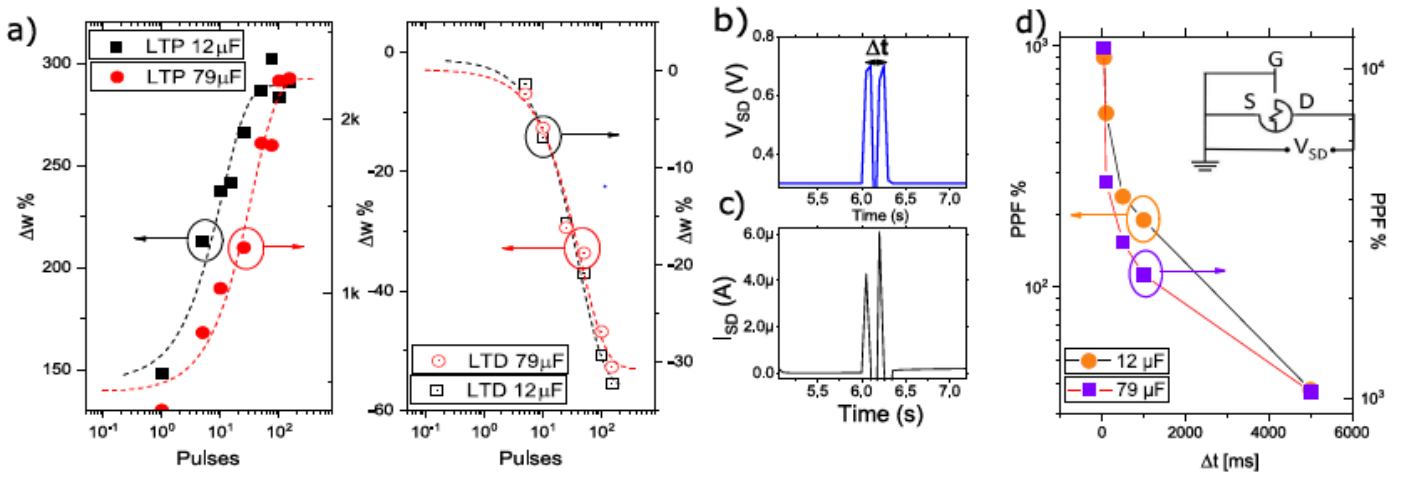

Figure 4: Synaptic properties of OMDs: Panel a) LTP and LTD test: OMDs emulates long term plasticity as a function of the number of delivered voltage spikes; panel b) voltage pulses and current output (panel c) used for the induction of the short term plasticity in devices. Panel d) PPF % as a function of the interval time Δt. In inset: circuit wiring diagram for operating the OMD for the emulation of synaptic functions

promotes the increasing of conductivity and results in the enhancement of the synaptic weight ($\Delta w = (I^f_{SD} - I^0_{SD})/I^0_{SD}$) as a function of the number of delivered stimuli (Figure 4a). Differently from it was reported in Ref.[45], this stimulation configuration does not result in a short term adaptation behaviour (in which Δw must be close to 0). This is attributable to the faster switching process of this type of memristive device whose internal conductivity state is sensible to 100 ms stimulation. However, this effect can be modulated by reducing the V_p and the Δt to values allowing this kind of slower transition between resisitive states. As a further demonstration, the number of pulses necessary for the reaching of the saturation is markedly reduced respect to the already mentioned work. The administration of negative voltage pulses (V_p=-200 mV,Δt=100 ms) results instead in a marked reduction of the synaptic weight. These two trends, in which the synaptic weight depends on the train of stimuli and on the number of delivered pulses, can be considered as the voltage based expressions of Long Term Potentiation and Depression of OMDs. However, a form of short term plasticity, namely paired-pulse facilitation (PPF), could be evoked in OMDs when delivering to the device two voltage spikes of 700 mV with different time intervals (from Δt = 50 *ms* to Δt = 5000 *ms* at 50 mV). As already mentioned, 300 mV voltage is the reading voltage for the correct estimation of the PPF%, whose definition is identical to the Δw one. OMD current response (Figure 4d) is the analogous of the biological paired-pulse facilitation in which the device temporally correlates two subsequent spikes on the basis of the Δt. Shorter is the interval between pulses and higher is the PPF %. Devices with different capacitive values show very similar neuromorphic behaviors which are, however, shifted to higher values in agreement with variations of $(R_{OFF} - R_{ON})/R_{ON}$ reported in Figure 3b. For the realization of integrated circuits mimicking different functions of biological neuronal networks, the possibility of implementing neuronal features in addition to synaptic functions, is a crucial aspect. Neurons in a biological network are responsible for the so called temporal or spatial integration which are mechanisms of eliciting postsynaptic potentials in the case of high frequency of unsynchronized presynaptic action potentials or in case of multiple spatial isolated synaptic inputs, respectively. We tested the integration abilities of OMDs following two distinct stimuli protocols, represented in Figure 5a and in Figure 5d respectively. To test the temporal summation, we applied to OMDs the voltage profile reported in Figure 5b in which an increasing number of voltage spikes of 700 mV amplitude are delivered with 100 ms time intervals. OMD current response (top panel of Figure 5b) and Figure 5c show clearly that an increasing number of inputs elicits proportionally the final current of the device, which thus, is able to integrate subsequent incoming spikes. This trend mimics well the temporal integration of biological neurons.

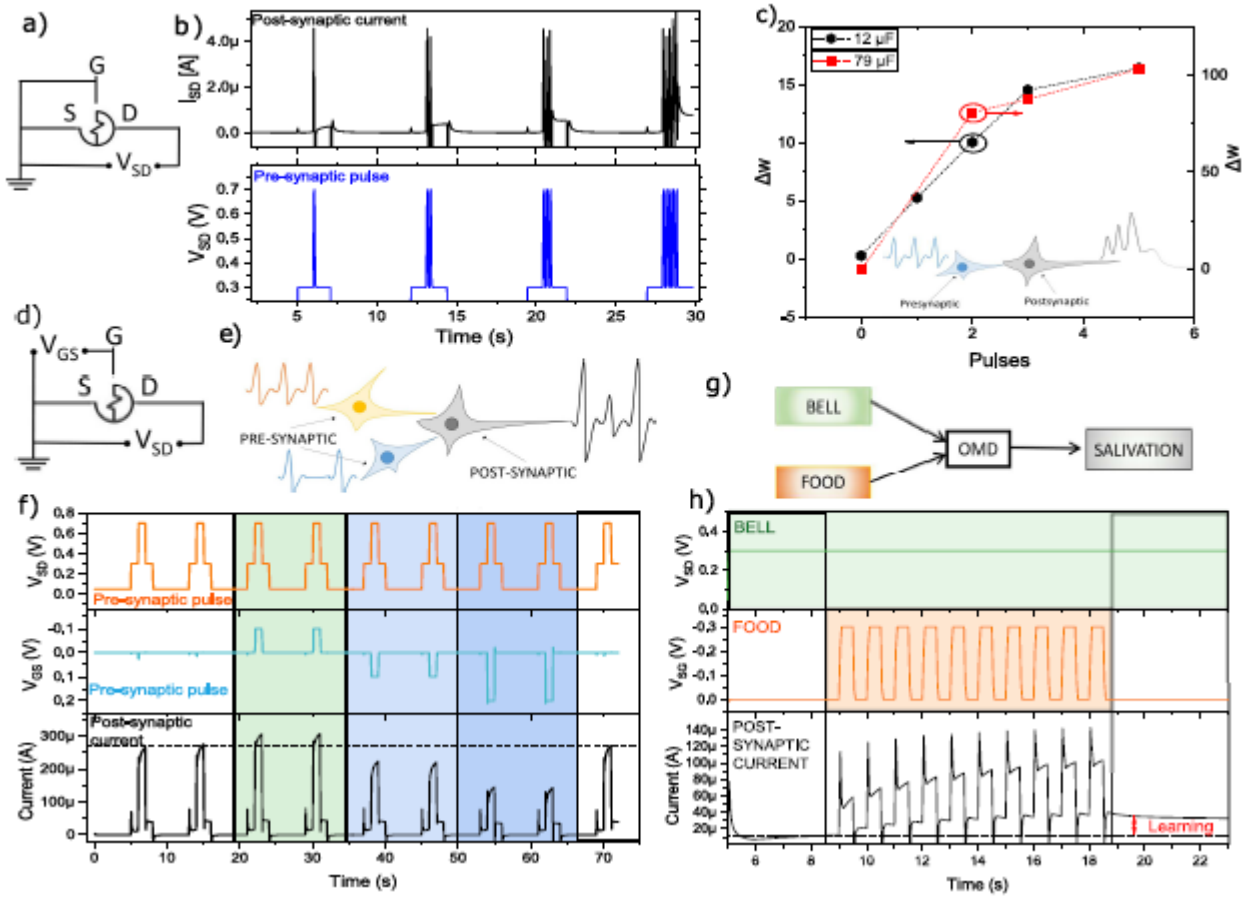

Figure 5: Spatio-temporal integration capabilities of OMDs: panel a) circuit wiring diagram for operating the OMD for the temporal integration function; panel b) current output (black curve) and voltage profile (blue curve) used for the temporal integration; panel c) Results of the temporal integration as a function of the number of received stimuli. panel d) circuit wiring diagram for operating the OMD for the spatial integration function; schematic (panel e) and results (panel f) of the spatial integration test: OMDs can integrate (bottom panel) two different "presynaptic" inputs (top and middle panels); schematic (panel g) and results (panel h) of the Pavlovian conditioning and permanent association test

To assess the possibility of spatial integration, we took advantage of the three terminals configuration that organic memristive devices naturally present. Presynaptic inputs are represented by the two bias applied to source and drain (V_{DS}) and gate and source (V_{GS}) electrodes (Figure 5e). Results of this test are shown in Figure 5f in which we considered 3 different scenarios of stimulations: (i) Presynaptic 1 delivers signals to postsynaptic cells, while Presynaptic 2 is silent; (ii) Presynaptic 1 and Presynaptic 2 deliver excitatory signals to postsynaptic cells; (iii) Presynaptic 1 delivers excitatory signals to postsynaptic cells and Presynaptic 2 inhibitory spikes. The protocol (i) (white panels in Figure 5f) produces in the device a stable response that represents the neuronal behaviour to the stimulation from a single afferent cell. In contrast, protocols (ii) and (iii) induce in OMDs a variation in the current response which results enhanced in the first case (green panels in Figure 5e) and depressed in the second (light blue panels in Figure 5e). The decrease is proportional to the intensity of the inhibitory input which is able to modulate the output current.

The direct consequence of the capability of OMDs to spatially and temporally integrate signals is the possibility of emulating the Pavlov's dog experiment (Figure 5g) with a single device (Figure 5h). In this experiment, a single OMD is exposed to a neutral signal (green panel-The bell sound) which initially cannot induce variations in the output current (bottom panel). The contemporary administration of a neutral plus an unconditional stimulus (orange panel- Food) conditions the device which starts associating the bell sound with the presence of food. After this conditioning phase, the neutral bell sound induces a conditioned response demonstrated by the variation in the final current level.

2.4 Bio-signal amplification

Considering the linear trend reported in Figure 2a and c, OMDs can modulate their sensing capabilities on the basis of the internal resistive state and channel volume. Furthermore, variations of the conductivity should affect the amplification capability of the device. To test this feature, we applied to device's gate electrode a simulated electrocardiogram (ECG) signal, while monitoring the PANI channel current with the reading voltage of 300 mV (Figure 6c). This is repeated after having modified the OMD conductivity with depressing and potentiating pulses. OMDs, depending on their internal resistance and on their geometrical aspect ratios (which affect the capacitance) can sense and amplify an ECG biosignal (Figure 6a and b). The role of the capacitance in the capability of detecting an incoming mV signal is confirmed in Figure 6a and b in which two OMDs with different capacitance values show a marked difference in their responses to ECG inputs, as expected from the linearity in Figure 2c. Devices with higher C have a higher signal to noise ratio (S/N ≈ 30dB). On the contrary, a low capacitance value results in a device output with lower S/N (S/N ≈ 10dB) and the need of a post-acquisition signal treatment to extract ECG classical features. The variation of device conductivity results in an increase or decrease of the S/N, which is mostly due to the gently amplification of the signal peak-to-peak amplitude, more than a noise reduction.
It is worth emphasizing that devices with higher capacitance values are able to resolve all main components of ECG (Figure 6d). Interestingly, high capacitance OMDs can easily distinguish a normal ECG from a pathological one, as it is clearly visible in Figure 6e-g where a normal ECG and two pathological signals are sensed with the device.

3 Conclusion

In summary, we have reported new evidences of the importance of the capacitance as parameter for the designing of different applications for OMDs. We also have shown, with a new class of OMDs (liquid based) that these devices can endure for more than 1000 cycles and can easily access to more than 50 different resistive states, equivalent to a 5.5 memory bits. In these devices, the relative ratio between low and high resistance depends on the capacitive values. In the perspective of building integrated systems for the contemporary processing of data coming from sensors, we revealed the potentialities of OMDs both as sensing elements and as neuromorphic analogue. Indeed, we demonstrated that a single PANI based OMD can mimic both synaptic functions, among which voltage dependant LTP/LTD and short term PPF. Moreover, a single device is able to implement neuronal spatio-temporal integration functions taking advantage of the three-terminals configuration. In this light, we have also demonstrated that OMD emulates the Pavlovian learning demonstrating associative memory. Furthermore, on the basis of their

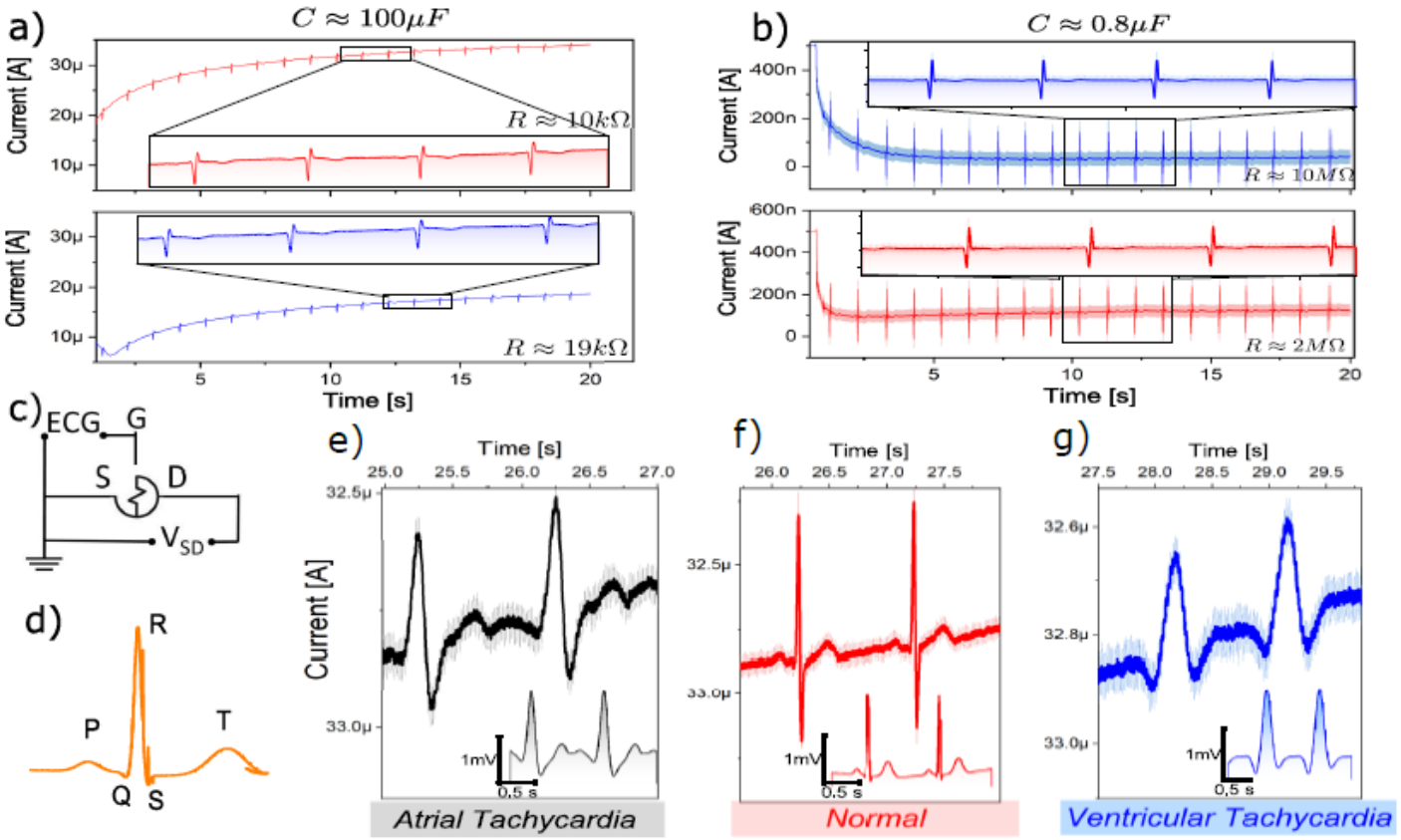

Figure 6: : Panel a) Response of high capacitance OMDs to ECG; panel b) Response of low capacitance OMDs to ECG; panel c) circuit wiring diagram for operating the OMD for bio-sensing; panel d) ECG main components: the P wave (the atria depolarization); the QRS complex (the depolarization of the ventricles);and the T wave, which represents the repolarization of the ventricles; Response of high capacitance OMDs to pathological (atrial and ventricular tachycardia- panel e and g) and normal ECG (panel f).

capacitive values, organic memristive devices can amplify and detect simulated ECG signals being able to recognize pathological features from normal cardiac signals.

4 Experimental Section

4.1 Device realization

Gold electrodes were deposited by e-beam evaporation (ULVAC EBX-14D) of Ti/Au film (thickness 10nm /100nm) on Si wafer (100) finished with 1 μm of thermal oxide, patterned by standard photolithography and wet etching as reported elsewhere [47]. PANI films were prepared spreading a PANI solution (0.1 mg/mL) of emeraldine base (Sigma Aldrich, Mw≈100.000) in 1-methyl-2-pyrrolidinone (Sigma Aldrich ACS reagent ≥ 99.0%) with the addition of 10% of Toluene (AnalaR NORMAPUR® ACS) on the air/water interface. The so obtained film is then deposited by means of the Langmuir-Schaefer technique onto a masked substrate [43, 45]. We prepared devices with different ratios L/W*d varying the number of transfer processes during the deposition (from nominal 20 layers to 60). As liquid electrolyte, we used 100-200 μL of HCl 1M.

4.2 Device characterization

Prepared samples were electrically characterized using two source measure units (NI PXIe-4138/9) controlled by a customized ad hoc LABVIEW code and analyzed and graphed by means of OriginLab software.

4.2.1 Preliminary characterizations

All OMDs have been initially characterized sweeping the V_{SD} between -0.1 V and 0.7 V, with steps of 0.01 V varying the scan rate of the measurement between 200 mV/s and 50 mV/s.

4.2.2 Capacitance and temporal response characterizations

I_{GS} vs V_{SD} curves, obtained as described in the previous section, have been used for extracting the polymeric thin film capacitance using the following equation: [39, 38]

(2) $$C = \frac{\int_V I_{GS}\, dV}{(V_2 - V_1) * \nu}$$

where $V_2 - V_1$ is the voltage range used for the measurement and v is the scan speed. We tested different scan speeds for every sample and we reported the averaged obtained values. For the calculation of the τ, OMDs were stimulated with a voltage pulse of 0.7 V, while monitoring the current. The so obtained I_{SD} is fitted using the formula $I_{SD}(t) = y_0 + A_1 e^{t-t_0/\tau 1} + A_2 e^{t-t_0/\tau 2}$. The value that we considered for our estimations is τ_1 which typically corresponds to the minimum values. Thickness nominal values must be corrected considering the not complete transfer of single monolayers during the deposition. To estimate the correct values, we considered the theoretic conductivity of the PANI thin film [32] ($\sigma_t = 0.1\ Scm^{-1}$) and we extracted the thickness using the formula:

(3) $$d = \frac{\sigma_t * L * I}{W * V}$$

4.2.3 Endurance and resistive states

In endurance tests, a sequence of voltage pulses (250 ms at 300 mV; 250 ms at 700 mV; 250 ms at 300 mV and 250 ms at -200 mV) was applied to OMDs. Intervals in which V_{SD} =300 mV correspond to ”reading” phases whose only purpose is the reading of the instantaneous resistivity of the device. 700 mV and -200 mV correspond instead to ”writing” voltages that modify internal conductivity of OMDs.

For the estimation of the total number of resistive states, we monitored the device current while applying to V_{SD} the profiles reported in the bottom panels of Figure 3c and d. For both, the reading phase consists in 1 s at 300 mV, while 5 s at 50 mV is used as reset between one stimulation and the following one. In the first case, a 5 s pulses at 400 mV, 500 mV, 600 mV and 700 mV was tested while in the second stimulation scheme, 100 ms, 500 ms, 1000 ms, 2000 ms, 5000 ms and 10000 ms pulses at 700 mV are used as inputs.
Then, we applied to OMDs a more dense stimulation routine in which a 1 s voltage pulses of amplitude $V^i_p = 0.3V + i * 0.01V$ is followed and preceded by 1 s of reading phase (300 mV). This test was limited to a maximum value of $V_p = 0.9\ V$ for preventing electrodes damaging and undesired reactions. For the estimation of the maximal number of states, we used as a discrimination tool the accuracy reported in the specifications of our electrical set up (National Instruments). Finally the temporal stability of selected resistive states was assessed applying to the device a routine similar to the one used for determining of the number of internal resistive states, but in which the last reading phase is extended to 500 s.

4.2.4 Neuromorphic characterizations

For the realization of LTP-LTD experiments, a sequence of 100 ms pulses (700 mV for LTP and -200 mV for LTD) separated by 100 ms interval at 300 mV was applied. Reading phases prior and after this train of stimuli are performed by applying 1 s pulses at 300 mV.
For the PPF test, two 100 ms pulses at 700 mV are progressively separated by 50 ms, 100 ms, 500 ms, 1000 ms and 5000 ms intervals at 50 mV. Conductivity variations are estimated in the reading phases at 300 mV before and after the two voltage spikes.
In the temporal integration test, we monitored the evolution of the conductivity before and after the delivering to OMD of short 700 mV pulses (100 ms) as a function of an increasing number of spikes. Between every acquisition, device conductivity has been reset to initial value with 50 mV bias. In the spatial integration and in the Pavlov’s dog experiments, we monitored the OMD current while applying different voltage pulses to V_{GS} and V_{DS}. In the first one, we applied 9 cycles of the following volt age sequence (5s at 50 mV, 1 s at 300 mV, 1 s at 700 mV and 1 s at 300 mV) as $V_{DS,}$ while pairs of 1 s pulses at -100 mV, 100 mV and 200 mV were used as V_{GS}. In the Pavlov’s dog experiment instead, a constant bias of 300 mV was used as V_{DS}, while a sequence of 10 500 ms pulses at -300 mV was used as food stimulus.

4.2.5 Bio-signal stimulus

V_{GS} simulated normal ECG signals (NI LabVIEW Biomedical Toolkit) with heart beat of 60 bpm and a maximal allowed amplitude of 3 mV were used as inputs to OMDs. To sense the effect of the internal resistance state on the amplification and sensing capabilities, sensing phases (in which V_{DS}= 300 mV) were alternated to potentiating (V_{DS}= 700 mV) and depressing phases (V_{DS}= -300 mV). To test the capability of OMDs to sense and amplify normal and pathological ECG signals, we employed ECG signals (NI Lab VIEW Biomedical Toolkit) with heart beat of 60 bpm and a maximal allowed amplitude of 2 mV. Collected data where then smoothed with the adjacent-averaging method for graphical purposes.

Acknowledgements
Authors want to thank the bilateral project ”Hardware realization of Reservoir computing and pattern recognition systems based on deterministic and stochastic organic memristive devices” financed by CNR in the framework of the joint collaboration between CNR and RFBR (Russia).

References

[1] E. R. van Doremaele, P. Gkoupidenis, Y. van de Burgt, *Journal of Materials Chemistry C* 2019, *7*, 41 12754.

[2] D. Purves, G. Augustine, D. Fitzpatrick, W. Hall, A. LaMantia, R. Mooney, L. White, M. Platt, *Neuroscience*, Oxford University Press, 2018.

[3] A. Bofill-i Petit, A. F. Murray, *IEEE Transactions on Neural Networks* 2004, *15*, 5 1296.

[4] G. Indiveri, B. Linares-Barranco, T. J. Hamilton, A. Van Schaik, R. Etienne-Cummings, T. Del bruck, S.-C. Liu, P. Dudek, P. H¨afliger, S. Renaud, et al., *Frontiers in neuroscience* 2011, *5* 73.

[5] G. Indiveri, E. Chicca, R. Douglas, *IEEE transactions on neural networks* 2006, *17*, 1 211.

[6] J. Tang, F. Yuan, X. Shen, Z. Wang, M. Rao, Y. He, Y. Sun, X. Li, W. Zhang, Y. Li, et al., *Ad vanced Materials* 2019, *31*, 49 1902761.

[7] Z. Wang, S. Joshi, S. Savel'ev, W. Song, R. Midya, Y. Li, M. Rao, P. Yan, S. Asapu, Y. Zhuo, et al., *Nature Electronics* 2018, *1*, 2 137.

[8] A. Beck, J. Bednorz, C. Gerber, C. Rossel, D. Widmer, *Applied Physics Letters* 2000, *77*, 1 139.

[9] K. Szot, W. Speier, G. Bihlmayer, R. Waser, *Nature materials* 2006, *5*, 4 312.

[10] R. Waser, M. Aono, *Nanoscience And Technology: A Collection of Reviews from Nature Journals* 2010, 158–165.

[11] L. O. Chua, S. M. Kang, *Proceedings of the IEEE* 1976, *64*, 2 209.

[12] J. Grollier, D. Querlioz, M. D. Stiles, *Proceedings of the IEEE* 2016, *104*, 10 2024.

[13] J. Grollier, D. Querlioz, K. Camsari, K. Everschor-Sitte, S. Fukami, M. D. Stiles, *Nature electronics* 2020, *3*, 7 360.

[14] M. Prezioso, F. Merrikh-Bayat, B. Hoskins, G. C. Adam, K. K. Likharev, D. B. Strukov, *Nature* 2015, *521*, 7550 61.

[15] D. B. Strukov, G. S. Snider, D. R. Stewart, R. S. Williams, *nature* 2008, *453*, 7191 80. [16] S. H. Jo,

T. Chang, I. Ebong, B. B. Bhadviya, P. Mazumder, W. Lu, *Nano letters* 2010, *10*, 4 1297.

[17] S. Battistoni, A. Verna, S. L. Marasso, M. Cocuzza, V. Erokhin, *physica status solidi (a)* 2020, *217*, 18 1900985.

[18] P. Gkoupidenis, N. Schaefer, X. Strakosas, J. A. Fairfield, G. G. Malliaras, *Applied Physics Letters* 2015, *107*, 26 263302.

[19] Y. van de Burgt, E. Lubberman, E. J. Fuller, S. T. Keene, G. C. Faria, S. Agarwal, M. J. Marinella, A. A. Talin, A. Salleo, *Nature materials* 2017, *16*, 4 414.

[20] Y.-N. Zhong, T. Wang, X. Gao, J.-L. Xu, S.-D. Wang, *Advanced Functional Materials* 2018, *28*, 22

1800854.

[21] S. Battistoni, C. Peruzzi, A. Verna, S. L. Marasso, M. Cocuzza, V. Erokhin, S. Iannotta, *Flexible and Printed Electronics* 2019, *4*, 4 044002.

[22] P. Gkoupidenis, N. Schaefer, B. Garlan, G. G. Malliaras, *Advanced Materials* 2015, *27*, 44 7176.

[23] T. Fu, X. Liu, H. Gao, J. E. Ward, X. Liu, B. Yin, Z. Wang, Y. Zhuo, D. J. Walker, J. J. Yang, et al., *Nature communications* 2020, *11*, 1 1.

[24] T. Chen, X. Wang, D. Hao, S. Dai, Q. Ou, J. Zhang, J. Huang, *Advanced Optical Materials* 2021, 2002030.

[25] Y. Choi, S. Oh, C. Qian, J.-H. Park, J. H. Cho, *Nature communications* 2020, *11*, 1 1.

[26] M. Di Lauro, A. De Salvo, G. C. Sebastianella, M. Bianchi, S. Carli, M. Murgia, L. Fadiga, F. Bis carini, *ACS Applied Electronic Materials* 2020, *2*, 7 1849.

[27] C. Qian, L.-a. Kong, J. Yang, Y. Gao, J. Sun, *Applied Physics Letters* 2017, *110*, 8 083302.

[28] H. Ling, N. Wang, A. Yang, Y. Liu, J. Song, F. Yan, *Advanced Materials Technologies* 2019, *4*, 9 1900471.

[29] S. Yamamoto, G. G. Malliaras, *ACS Applied Electronic Materials* 2020, *2*, 7 2224.

[30] Q. Duan, Z. Jing, X. Zou, Y. Wang, K. Yang, T. Zhang, S. Wu, R. Huang, Y. Yang, *Nature com munications* 2020, *11*, 1 1.

[31] J. Lacroix, K. Kanazawa, A. Diaz, *Journal of the electrochemical society* 1989, *136*, 5 1308.

[32] A. Dhanabalan, R. Dabke, N. P. Kumar, S. Talwar, S. Major, R. Lal, A. Contractor, *Langmuir* 1997, *13*, 16 4395.

[33] S. Battistoni, R. Sajapin, V. Erokhin, A. Verna, M. Cocuzza, S. L. Marasso, S. Iannotta, *Chaos, Solitons & Fractals* 2020, *141* 110319.

[34] D. Lapkin, A. Emelyanov, V. Demin, V. Erokhin, L. Feigin, P. Kashkarov, M. Kovalchuk, *Applied Physics Letters* 2018, *112*, 4 043302.

[35] F. Pincella, P. Camorani, V. Erokhin, *Applied Physics A* 2011, *104*, 4 1039.

[36] M. K. Ram, M. Adami, M. Sartore, M. Salerno, S. Paddeu, C. Nicolini, *Synthetic metals* 1999, *100*, 3 249.

[37] S. Battistoni, V. Erokhin, S. Iannotta, *Neural plasticity* 2017, *2017*.

[38] J. Scotto, W. A. Marmisoll´e, D. Posadas, *Journal of Solid State Electrochemistry* 2019, *23*, 7 1947.

[39] A. Kellenberger, D. Ambros, N. Plesu, *Int. J. Electrochem. Sci* 2014, *9*, 12 6821. [40] L. Mao, M. Li,

J. Xue, J. Wang, *RSC advances* 2016, *6*, 4 2951.

[41] Y. Wang, X. Yang, A. G. Pandolfo, J. Ding, D. Li, *Advanced Energy Materials* 2016, *6*, 11 1600185.

[42] J. Rivnay, P. Leleux, M. Ferro, M. Sessolo, A. Williamson, D. A. Koutsouras, D. Khodagholy, M. Ramuz, X. Strakosas, R. M. Owens, et al., *Science advances* 2015, *1*, 4 e1400251.

[43] S. Battistoni, A. Dimonte, V. Erokhin, *Organic Electronics* 2016, *38* 79.

[44] S. Stathopoulos, A. Khiat, M. Trapatseli, S. Cortese, A. Serb, I. Valov, T. Prodromakis, *Scientific reports* 2017, *7*, 1 1.

[45] S. Battistoni, V. Erokhin, S. Iannotta, *Organic Electronics* 2019, *65* 434.

[46] N. V. Prudnikov, D. A. Lapkin, A. V. Emelyanov, A. A. Minnekhanov, Y. N. Malakhova, S. N. Chvalun, V. A. Demin, V. V. Erokhin, *Journal of Physics D: Applied Physics* 2020, *53*, 41 414001.

[47] V. Preziosi, M. Barra, A. Perazzo, G. Tarabella, A. Romeo, S. Marasso, P. D'Angelo, S. Iannotta,

A. Cassinese, S. Guido, *Journal of Materials Chemistry C* 2017, *5*, 8 2056.
REFERENCES

Table of Contents

Organic memristive devices are polymeric based devices showing neuromorphic and sensing capabilities. Here we present a vast range of emulative abilities who span from the mimicking of synaptic properties to neuronal functions of spatio temporal integration. Moreover, the same device can efficiently sense ECG signals. This combination of neuromorphic properties, memorization capabilities and sensing abilities suggests their use in integrated circuits with local processing of sensors outputs.